Compositional cyclicity in a pyroxenitic layer from the Main Zone of the Western Bushveld Complex: evidence for repeated magma influx

ANDREW A. MITCHELL

Department of Geology, University of Durban-Westville, Private Bag X54001, Durban 4000, South Africa

Abstract

Lacking the pronounced modal layering of the underlying Critical Zone, the Main Zone of the Bushveld Complex nevertheless displays well-developed cryptic layering, expressed in a series of iron-enrichment trends, each defining a unit of the order of 100 to 200 m thick. At the base of one such unit, 1100 m above the Main Zone – Critical Zone contact, a 10 m thick pyroxenitic layer was intersected in an exploration borehole from the southern sector of the western Bushveld.

Within the pyroxenitic layer, mineral chemistry defines a series of five cycles of upward Mg and Cr enrichment in pyroxenes, and Ca enrichment in plagioclase. The mineral chemistry, supported by textural evidence, suggests the influx of successive surges of magma. Sustained streaming of magma gave rise to adcumulate textures in the central portion of each cycle, with orthocumulate textures at bases and tops of cycles representing waxing and waning stages of magma surges.

KEYWORDS: Bushveld Complex, Main Zone, pyroxenite, magma influx, compositional cyclicity.

Introduction

THE Main Zone (MZ) of the Bushveld Complex is generally perceived to be a monotonous sequence of gabbroic rocks, displaying a trend of almost uninterrupted iron-enrichment over a stratigraphic thickness in excess of 2000 m. This led Wager and Brown (1968) to include the MZ as part of their postulated "differentiation stage" of the complex, within which little or no new magma addition occurred. Sharpe (1985) reinforced this view by suggesting, on the basis of Sr isotope systematics, that there was a massive influx of magma at approximately the level of the Merensky Reef. This single magma influx was inferred to have been interposed between the crystalline substrate and the supernatant liquid, and to have crystallized to form the approximately 2000 m thick succession between the top of the Upper Critical Zone and the base of the Pyroxenite Marker.

Mitchell (1990*a*) and Mitchell and Scoon (1991) placed the base of the Main Zone above the Giant Mottled Anorthosite, at the top of the Bastard Unit, and assigned the Main Zone succession up to the Pyroxenite Marker to the Lower Main Zone (LMZ). Primarily on the basis of mineral chemistry, Mitchell (op. cit.) suggested that fractionation in the LMZ was not continuous, but was punctuated by several small influxes of fresh magma, each producing a minor reversal in the general trend of differentiation. Recently published Sr isotope data (Kruger, 1994) support the multiple influx hypothesis, as do grain size variation trends in plagioclase (Maier and Mitchell, 1995).

In a borehole core from the southern sector of the Western Bushveld, Mitchell (1990*b*) identified several successive cycles of magma influx and differentiation on the basis of the Mg# of low-Ca pyroxene. The base of one such cycle, designated unit G-IX, is marked by a pyroxenite layer approximately 10 m thick. Within this pyroxenite layer, compositional cyclicity on a metre scale is illustrated by variations in the Mg# and Cr_2O_3 content of low-Ca pyroxene and augite, as well as the Ca content of plagioclase.

Throughout this study, stratigraphic heights in the Main Zone are quoted in metres above the base of the Main Zone, and were measured directly off the

Mineralogical Magazine, February 1996, Vol. 60, pp. 149–161

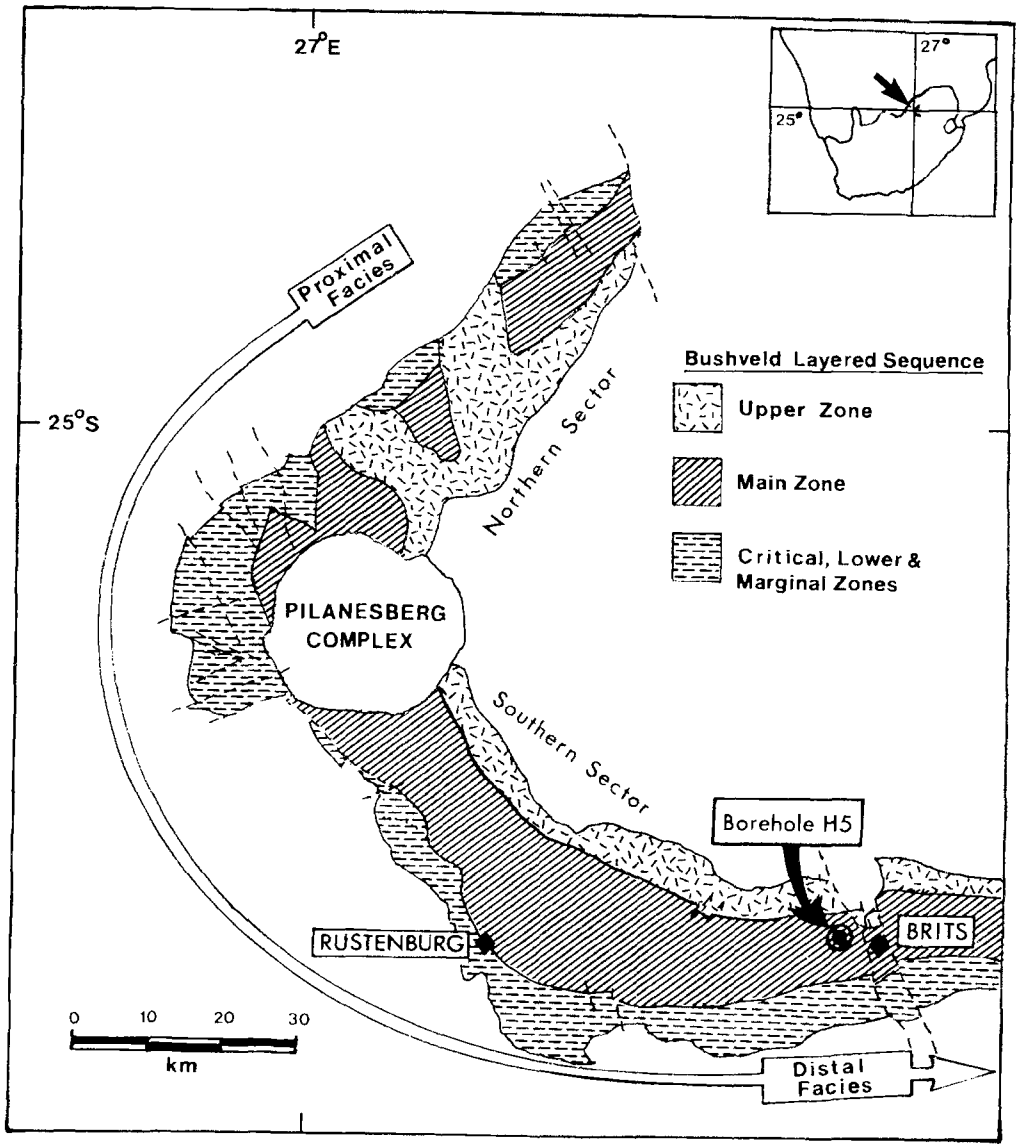

FIG. 1. Simplified sketch map of the western Bushveld Complex, showing the location of borehole H5.

borehole core, with no correction for the average regional dip of 15° in the Brits area.

Geological setting

Borehole H5, which is situated approximately 5 km west of the town of Brits, in the southern sector of the western Bushveld Complex (Fig. 1), intersected slightly less than 1400 m of LMZ gabbronorite and norite before passing into the Upper Critical Zone. Approximately 1100 m above the base of the MZ, the H5 succession contains a melanocratic, pyroxenite-dominated layer, approximately 10 m thick. No similar layers are present in other recorded MZ borehole intersections, either from the immediate vicinity or from the western Bushveld at large. This

tends to indicate lateral impersistence of the layer, although it must be stated that borehole coverage of the upper part of the LMZ is very limited. Allied to the extremely poor outcrop in the western Bushveld, this makes tracing the layer along strike impossible.

On the basis of its chemistry and mineralogy, the pyroxenite layer is not part of the "iron-rich ultramafic pegmatite (IRUP) suite" (Scoon and Mitchell, 1994). Furthermore, its position in the stratigraphy, allied to its lateral impersistence, discounts its interpretation as a correlative of the Pyroxenite Marker (Cawthorn *et al.*, 1991), the probable stratigraphic position of which is at least 100m above the top of the sequence intersected by borehole H5. The layer may, however, correlate with a feldspathic pyroxenite layer recorded by Quadling and Cawthorn (1994) at an apparently similar level in the MZ of the eastern Bushveld.

The pyroxenite layer occurs within typical LMZ gabbronorites, in which orthopyroxene or inverted pigeonite constitutes approximately 25% of the volume of the rock, augite 15%, and plagioclase usually in excess of 60%. The layer is situated at the base of one of a series of successive low-Ca pyroxene iron-enrichment trends (unit G-IX) within the LMZ in this part of the Bushveld (Fig. 2), and is referred to in this work as the G-IX pyroxenite layer. Whereas most of the LMZ units in the H5 succession have strongly Fe-enriched tops (e.g. units G-VI, G-VII, G-IX: Fig. 2), the unit forming the footwall to the G-IX pyroxenite (unit G-VIII) does not, perhaps indicating a truncated fractionation cycle.

Borehole H5 is situated within the postulated distal facies of the western Bushveld (Eales *et al.*, 1988, 1993, 1994; Scoon and Teigler, 1994). This is reflected in the fact that the equivalent of the

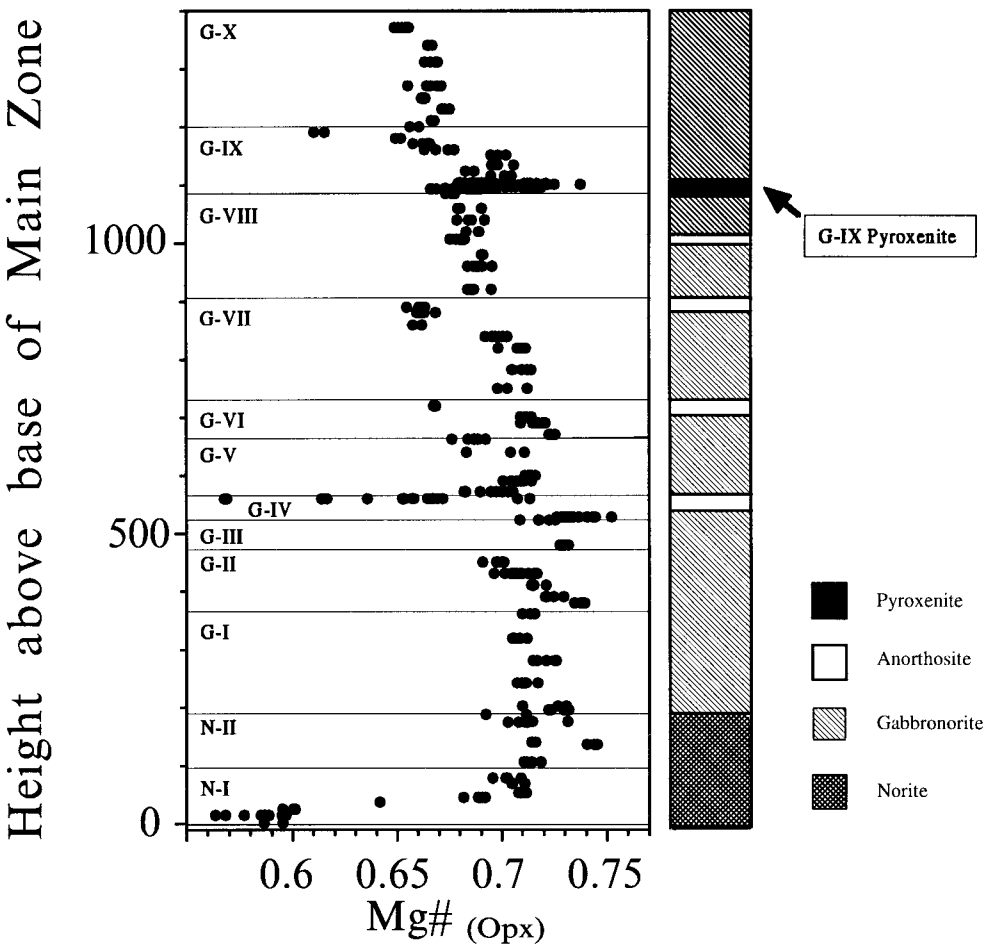

FIG. 2. Plot of low-Ca pyroxene Mg# through the Main Zone succession in borehole H5, illustrating the position of the G-IX pyroxenite layer at the base of unit G-IX.

TABLE 1. Summarized petrographic and mineral chemical data for the G-1X pyroxenite

Sample	Strat. height	Modal mineralogy Plag	Opx	Aug	Other	Max. grn. Opx	Aug	Mg#opx	Mg#aug	An
Gabbronorite hangingwall										
320	1103.2	79.7	18.7	1.6	0.0	5.19	1.11	0.680	0.777	0.702
Cycle V										
330	1102.6	33.0	32.0	34.3	0.7	11.11	1.85	0.721	0.775	0.674
340	1101.6	27.8	22.2	48.6	1.4	6.85	4.44	0.738	0.770	0.654
350	1101.0	2.7	7.5	89.8	0.0	5.56	4.44	0.720	0.762	0.633
360	1100.6	1.5	26.2	72.3	0.0	7.41	10.37	0.722	0.772	0.647
380	1100.0	3.5	62.5	34.0	1.0	7.04	3.15	0.704	0.787	0.563
Cycle IV										
390	1099.8	30.2	45.8	24.0	0.0	2.22	1.48	0.714	0.786	0.629
400	1099.4	0.5	57.2	32.2	9.9	8.15	3.52	0.693	0.770	0.507
410	1099.2	33.5	55.5	11.0	0.0	5.93	4.44	0.708	0.762	0.651
Cycle III										
420	1098.8	29.8	33.2	37.0	0.0	9.26	0.74	0.715	0.777	0.672
440	1098.4	0.5	24.3	74.5	0.7	9.26	7.04	0.719	0.783	0.616
460	1098.1	5.0	37.3	57.7	1.0	5.93	3.52	0.712	0.760	0.613
490	1097.7	2.2	53.3	43.5	1.0	5.19	3.70	0.710	0.777	0.600
Cycle II										
510	1097.3	15.5	26.0	58.5	0.0	5.19	3.15	0.714	0.779	0.656
530	1096.8	33.5	44.7	21.8	0.0	4.81	1.48	0.710	0.762	0.661
540	1096.6	2.0	65.2	31.3	1.0	6.30	6.30	0.698	0.773	0.662
550	1096.4	4.8	56.5	34.2	4.5	5.56	5.19	0.697	0.762	0.639
570	1096.0	24.8	60.2	14.8	0.2	5.19	2.96	0.694	0.767	0.597
Cycle I										
580	1095.7	29.5	44.7	25.8	0.0	2.22	1.11	0.719	0.794	0.680
581	1095.4	3.3	55.0	39.2	2.5	7.45	7.31	0.703	0.767	0.590
590	1095.0	29.8	39.5	30.0	0.7	4.44	2.96	0.692	0.758	0.665
620	1094.5	4.0	60.7	32.8	2.5	5.19	4.07	0.697	0.775	0.661
630	1094.3	39.8	42.2	18.0	0.0	4.07	2.04	0.698	0.768	0.632
650	1093.8	4.5	36.7	58.8	0.0	4.81	4.07	0.690	0.762	0.617
Gabbronorite footwall										
660	1093.4	72.8	14.5	12.6	0.0	4.00	1.82	0.680	0.763	0.689

Strat. Height is stratigraphic height above the base of the Main Zone.
Max. grn. is maximum grain diameter (measured in mm).
Mg#opx and Mg#aug are the atomic ratio Mg/(Mg+Fe) for low-Ca pyroxene and augite, respectively, and are the maximum values for each sample.
An is the maximum ratio An/(An+Ab) for each sample.

1100 m thick succession up to the base of unit G-IX in borehole H5 (Fig. 2) is of the order of 1570 m thick in the proximal northern sector of the western Bushveld (Mitchell, 1990*a*), and approximately 1460 m thick at Rustenburg (Meyer, 1969), which represents an intermediate facies. It is perhaps also a function of its location in the distal facies that the H5 succession displays better developed fractionation trends (Fig. 2) than those illustrated by Mitchell (1990*a*) from Rustenburg Platinum Mines Union Section, in the postulated proximal facies of the western Bushveld.

Analytical methods

Modal analyses, utilizing at least 800 points per thin section, were performed using the computerized stage control and data reduction techniques of Dunlevey and Mitchell (1994). Electron microprobe analyses of plagioclase and pyroxene were performed on a JEOL CXA-733 Superprobe at Rhodes University, Grahamstown, operated at 15kV, with a 25nA specimen current measured on the Faraday cage. Analytical precision (reproducibility) of the electron microprobe data, tested on the basis of ten closely spaced analyses in the central domain of the various phases, yielded a coefficient of variation of 0.19% for Mg# in orthopyroxene, and 0.3% for An content of plagioclase. Electron backscatter images and semi-quantitative characterizations of oxide and sulphide phases were obtained from a JEOL 6100 scanning electron microscope, equipped with a NORAN Voyager EDS system, at the University of Durban-Westville.

Petrography

The G-IX pyroxenite layer varies in modal mineralogy from orthopyroxenite, through websterite, to clinopyroxenite. In addition the modal proportion of intercumulus plagioclase, although usually less than 5%, is highly variable in the range 0.5 to 40 volume % (Table 1). The tops, and sometimes also the bases, of cycles have orthocumulate textures, with elevated intercumulus plagioclase contents. Adcumulates of augite and low-Ca pyroxene, with less than 5% intercumulus plagioclase, occur in the centres, and sometimes at the bases, of cycles.

Texturally, the succession is highly complex, but a central theme, particularly at the bases and tops of cycles, is the evidence of extreme disequilibrium. In

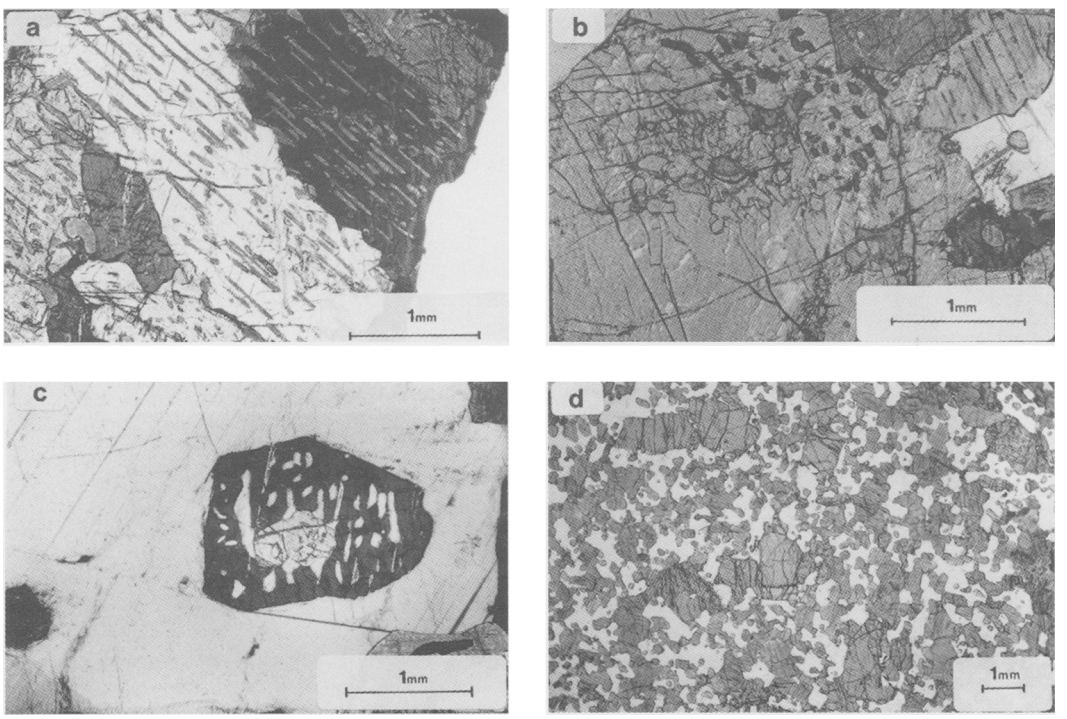

FIG. 3. (*a*) Augite exsolution lamellae in parallel orientation over several contiguous grains of low-Ca pyroxene: sample 570, at the base of cycle II(crossed polars). (*b*) The core of a low-Ca pyroxene grain displays augite exsolution, and is surrounded by exsolution-free pyroxene: sample 590, cycle I (crossed polars). (*c*) An early generation of low-Ca pyroxene is mantled by a later generation in a different orientation. Both generations have exsolved augite: sample 410, cycle IV (crossed polars). (*d*) A common texture in more plagioclase-rich lithologies is the inclusion of small, rounded and embayed augite grains and larger low-Ca pyroxene grains in poikilitic grains of intercumulus plagioclase: sample 420, cycle III (plane-polarized light).

the basal part of cycle II, orthopyroxene grains display exsolution blebs of augite in parallel orientation over several contiguous grains (sample 520: Fig. 3*a*). In sample 410, at the base of cycle IV, overgrowths of successive generations of low-Ca pyroxene are evident in several grains. In some grains, small, ovoid areas containing augite exsolution blebs within a larger, exsolution-free orthopyroxene grain attest to orthopyroxene overgrowth on a pre-existing grain of inverted pigeonite (Fig. 3*b*). In a smaller grain, enclosed by poikilitic intercumulus plagioclase, a rounded core of inverted pigeonite is surrounded by a later generation of inverted pigeonite in a different optical orientation (Fig. 3*c*).

At the tops of cycles I and III, there is an extreme development of a texture that is particularly evident at the top of each cycle, in which small, rounded and embayed grains of augite and significantly larger and less rounded grains of low-Ca pyroxene are poikilitically included in intercumulus plagioclase that is optically continuous over areas of ± 3 mm on average. This texture is illustrated by sample 420, from the top of cycle III (Fig. 3*d*). Another feature of sample 420 is that where augite grains are partially resorbed, thick '001' exsolution lamellae of low-Ca pyroxene (pigeonite) are preserved, and extend into, and sometimes right across, areas of intercumulus plagioclase (Fig. 4). Subsequent, thinner, '001' and '100' exsolution lamellae do not extend into intercumulus spaces. Robinson et al. (1977) estimated that coarse '001' exsolution lamellae in augite from Bushveld Main Zone gabbro formed at temperatures around 1000°C, whilst subsequent, thinner '001' lamellae formed at significantly lower temperatures (850° to 560°C).

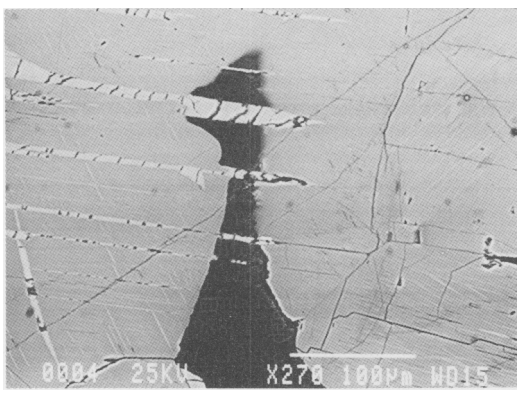

FIG. 4. Electron backscatter image of low-Ca pyroxene lamellae, exsolved from augite, extending into and across areas of intercumulus plagioclase (sample 420, cycle III). Plagioclase is black, augite mid-grey, and low-Ca pyroxene pale grey.

Apart from being included in intercumulus plagioclase, rounded and embayed grains of augite also occur as inclusions in low-Ca pyroxene throughout the G-IX pyroxenite succession. Embayed plagioclase inclusions in low-Ca pyroxene, as described by Eales *et al.* (1991), occur only in the uppermost sample (330) of cycle V, where they are abundant in large (11 mm diameter) cumulus low-Ca pyroxenes.

Accessory minerals included under the label 'other' in Table 1 are dominated by interstitial quartz and late-stage biotite. There is minor replacement of plagioclase by chlorite and clinozoisite in some samples. Apatite is a rare accessory mineral in samples 340, 550 and 620, where it occurs in association with quartz.

Opaque minerals are rare and generally late-stage components of the rocks. In most cases sulphides, usually predominantly chalcopyrite, are more common than oxides. Chalcopyrite occurs enclosed in either pyroxenes or plagioclase, and may in some cases be accompanied by tiny grains (<10 μm) of other sulphides, (e.g. sphalerite and pentlandite in sample 550, galena in sample 540) and even, in isolated cases, by tiny (<2 μm) PGM grains [cooperite (PtS) in sample 490; an Os-Ir-Ru-As-S phase associated with chalcopyrite in sample 510; a Pt-Pd-Te-As phase associated with chalcopyrite in sample 540]. In some samples, late-stage pyrite occurs at the interface between cumulus pyroxene and intercumulus plagioclase (Fig. 5*a*). Pyrite may also occur parallel to low-Ca pyroxene exsolution lamellae in augite (Fig. 5*b*). Late-stage ilmenite is the most common oxide phase, usually occurring in association with interstitial quartz (Fig. 5*c*). In some samples, late-stage magnetite occurs along fractures in augite, also infiltrating parallel to exsolution lamellae in augite (Fig. 5*d*). Small (<20 μm) Cr spinel grains were identified in samples 380, 400, 420, 460 and 580. A Cr spinel grain in sample 580 (top of cycle I), enclosed in low-Ca pyroxene, contains 37% Cr_2O_3, whereas a small Cr-spinel grain from sample 400, partially enclosed by ilmenite, contains 18% Cr_2O_3. In other samples, Cr-spinel compositions range between these two extremes.

Compositional variations within the pyroxenite layer

Compositional variations within the pyroxenite layer are illustrated by plots of Mg#, Cr_2O_3 and the Cr/Al ratio *vs.* stratigraphic height for both low-Ca pyroxene and augite (Figs. 6, 7), and the An/(An+Ab) ratio of plagioclase (Fig. 8). Disequilibrium processes are evident from the petrography of the rocks, indicating the possibility

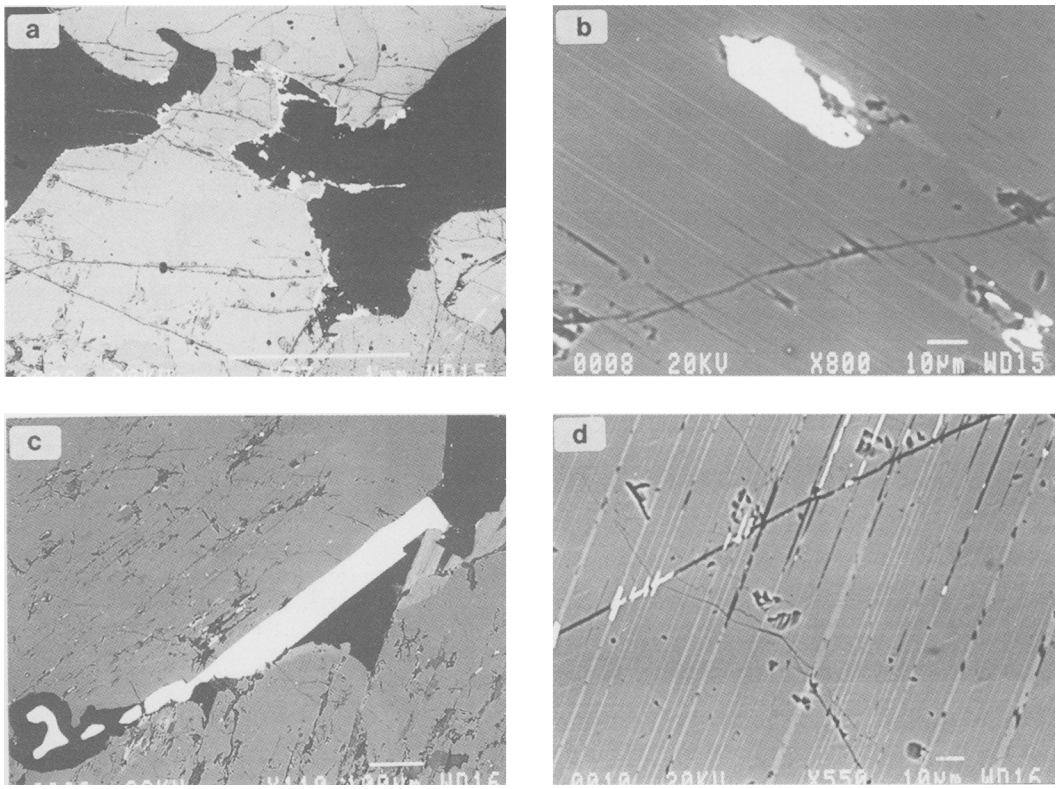

FIG. 5. Electron backscatter images of ore minerals: (*a*) Pyrite (white) at the interface between plagioclase (black) and augite (pale grey) in sample 340. (*b*) Pyrite (white) parallel to cleavage and hypersthene exsolution lamellae in augite (sample 440). (*c*) Acicular ilmenite (white) associated with interstitial quartz (black) (sample 380). (*d*) Magnetite (white) along fracture and cleavage in augite (sample 350).

of mixed parentages for the pyroxenes. This is one of the reasons why maximum values of the Mg# and Cr_2O_3 contents of pyroxene, and the An content of plagioclase, are recorded in Table 1, rather than mean compositions. Another, more practical, reason is that the number of analyses of each mineral varies from three to twelve from sample to sample, making the mean a statistically invalid value.

In both pyroxenes, the Cr_2O_3 and Cr/Al data display particularly coherent trends. The pyroxenes at the base of each of the five cycles are depleted in chromium relative to the top of the preceding cycle. The tops of each of the cycles, except cycle V, are significantly enriched in chromium, this being particularly so of cycles I and III. The pyroxenite layer is enriched in chromium relative to both the underlying and the overlying gabbronorite, and the gabbronorite in the hangingwall is enriched in chromium relative to the footwall.

Augite, and to a lesser extent low-Ca pyroxene, display fairly wide within-sample variations in Mg#. In a gross sense, however, the Mg# of both pyroxenes follows the pattern of chromium variation, the bases of the cycles being Fe-enriched, and the tops being relatively Mg-rich. Although the Mg# of augite in the immediate hangingwall and footwall gabbronorites is little different from that in the pyroxenite layer, orthopyroxene is consistently more magnesian in the pyroxenite layer than in the underlying and overlying gabbronorite.

Except in cycle I, within-sample compositional ranges in plagioclase are surprisingly small in the pyroxenite layer, especially since plagioclase displays extremely wide within-sample compositional variations throughout most of the Bushveld Complex stratigraphic succession (Mitchell, 1990*a*; Eales *et al.*, 1990). This is probably because plagioclase occurs only as an intercumulus phase in

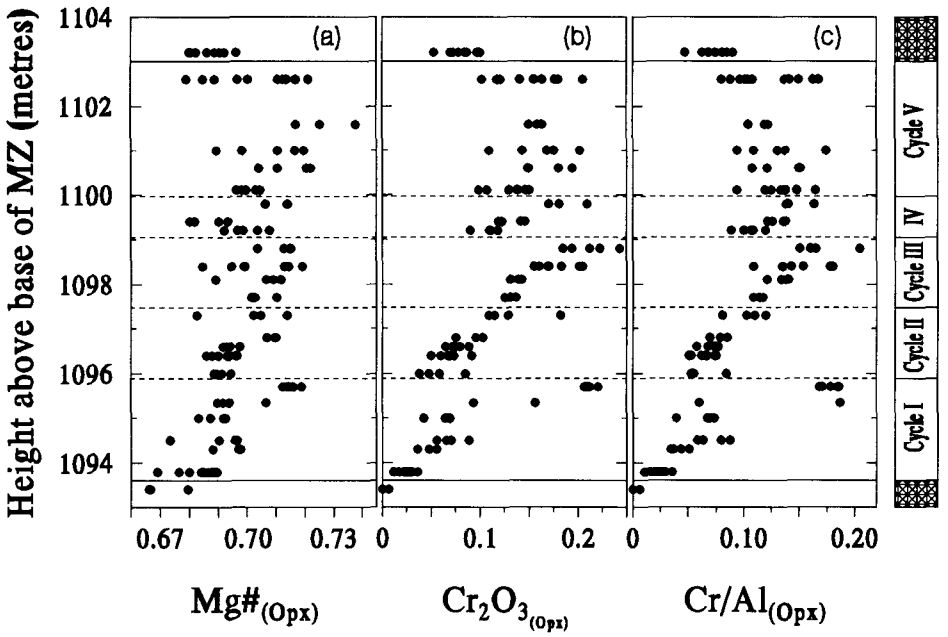

FIG. 6. Compositional trends in low-Ca pyroxene through the G-IX pyroxenite layer, illustrating subdivision into five cycles: (*a*) the magnesium number [Mg# = atomic ratio Mg/(Mg+Fe)]. (*b*) Weight percent Cr_2O_3. (*c*) The atomic ratio Cr/Al.

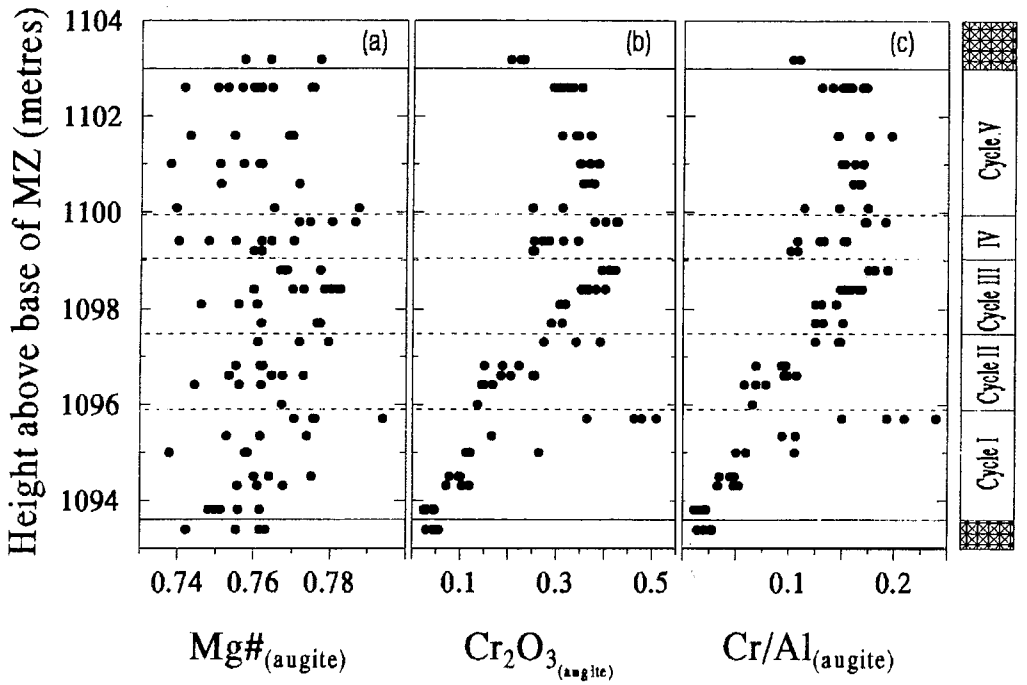

FIG. 7. Compositional trends in augite through the G-IX pyroxenite layer: (*a*) the magnesium number [Mg# = atomic ratio Mg/(Mg+Fe)]. (*b*) Weight percent Cr_2O_3. (*c*) The atomic ratio Cr/Al.

the pyroxenite, with no petrographic evidence for complex mixtures of different lineages of plagioclase identified by Eales *et al.* (1991) in the Critical Zone. The An/(An+Ab) ratio of plagioclase echoes the trends defined by the pyroxene data, basal samples of cycles having evolved (Na-enriched) compositions, and samples at the tops of cycles being relatively calcic (Fig. 8). There is a particularly sharp reversal to more sodic compositions across the boundary between cycles II and III. This latter boundary is, in fact, defined primarily on the basis of plagioclase compositions, with only a minor inflection in pyroxene compositions. Sample 490, at the base of cycle III, is an adcumulate containing only 2.2% modal intercumulus plagioclase. Overall, the composition of the intercumulus plagioclase in the pyroxenite layer is more sodic than the cumulus plagioclase in the overlying and underlying gabbronorites. This is in line with the findings of Eales *et al.* (1990) that intercumulus plagioclase is of the order of 10% more sodic than associated cumulus varieties in the Upper Critical Zone.

Summary

The G-IX pyroxenite layer occurs at a height of 1100 m above the base of the LMZ succession in borehole H5, which is situated in the postulated distal facies of the southern sector of the western Bushveld Complex (Eales *et al.*, 1993; Scoon and Teigler, 1994). The pyroxenite layer appears to be laterally impersistent, even on a local scale. It does, however, occur at the base of a pronounced differentiation trend in the upper part of the LMZ, which correlates with a similar trend in the LMZ succession of the northern sector of the western Bushveld (Mitchell, 1986; 1990*a*). There are several successive Fe-enrichment cycles in the H5 sequence, with the one in the footwall of the pyroxenite giving some indication of truncation.

The pyroxenite layer is subdivisible into a series of five cycles of reversed differentiation, each of the order of 1 m to 3 m thick. The base of each successive cycle exhibits significant Fe-enrichment and Cr-depletion in the pyroxenes, and Na-enrichment in plagioclase, relative to the top of the underlying cycle. The top of each cycle, by contrast, displays enrichment of Cr and Mg in pyroxenes, and Ca in plagioclase (the uppermost cycle V being an exception). The boundary between cycles II and III appears superficially to be rather tenuously defined, particularly as regards pyroxene chemistry, although there is a distinct inflection in plagioclase chemistry across the boundary.

Within-sample variations in Cr_2O_3 content of both pyroxenes is fairly tightly constrained, but within-sample variations in Mg# of the pyroxenes is fairly wide, this being particularly so in the case of augite. Within-sample ranges in the An content of plagioclase are relatively small by comparison with much of the Upper Critical Zone and LMZ succession. This is perhaps due to the fact that all the plagioclase in the G-IX pyroxenite layer is intercumulus, whereas plagioclase grains in other parts of the Bushveld succession show evidence of mixed parentage.

There is no obvious correlation between the mineral chemistry and the physical appearance of the rocks, as expressed in grain size and modal variations. The modal plagioclase content is less than 5% through most of the layer, but may be as high as 40% in some samples. Plagioclase is invariably intercumulus.

The G-IX pyroxenite differs from the orthopyroxene-dominated pyroxenite cumulates of the UCZ and the lower part of the LMZ in that the modal augite content of the layer is high, ranging from 11% to 90%. In all samples, the maximum grain size of augite is less than that of low-Ca pyroxene. Augite grains are smallest when the plagioclase content of the rock is high, especially at the tops of cycles I, III, IV and V. Under these circumstances, augite forms small, rounded and embayed grains enclosed in large,

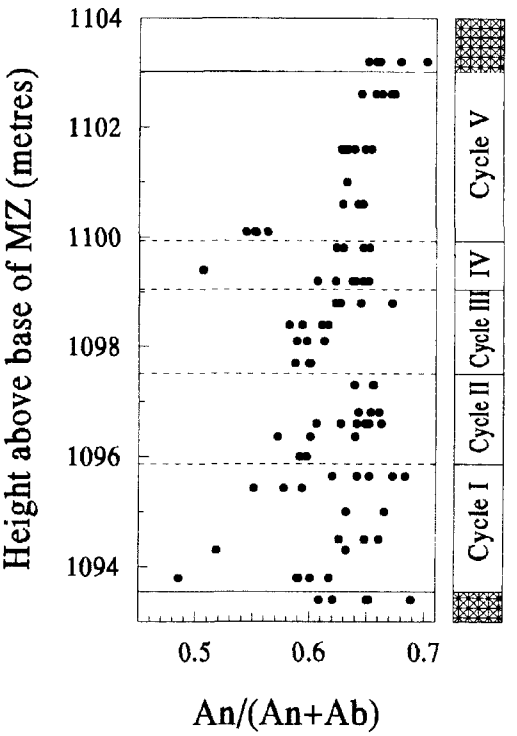

FIG. 8. The An/(An+Ab) ratio of plagioclase in the G-IX pyroxenite layer.

poikilitic, intercumulus plagioclase grains. A particularly extreme case of embayment of augite occurs in sample 420, at the top of cycle III, where embayments in augite grains leave exsolution lamellae of low-Ca pyroxene projecting across intercumulus plagioclase infillings (Fig. 4). Rounded grains of augite occur not only in plagioclase, but also in low-Ca pyroxene, throughout the G-IX pyroxenite.

At the base of cycle IV, sample 410 contains rounded grains of pyroxene (particularly low-Ca pyroxene) within overgrowths of a later generation of low-Ca pyroxene (Fig. 3*c*). At the base of cycle II, augite exsolution lamellae are in optical continuity over several contiguous grains of low-Ca pyroxene, even though the host grains are not in optical continuity (Fig. 3*a*).

The uppermost cycle of the pyroxenite (cycle V) displays slight basal iron-enrichment and Cr-depletion in the pyroxenes, and relatively substantial basal Na-enrichment in plagioclase. Unlike the underlying cycles, there is no Mg and Cr-enrichment of pyroxene, or Ca-enrichment of plagioclase, at the top of cycle V. The uppermost sample of cycle V is extremely coarse-grained, with grains of low-Ca pyroxene attaining a maximum diameter of 11 mm.

Discussion

The most conspicuous feature of the G-IX pyroxenite is the presence, within a 10 m stratigraphic interval, of five cycles of reversed fractionation. This is illustrated not only by the Mg# and Cr_2O_3 content of apparently cumulus orthopyroxene and augite, but also by the Ca content of invariably intercumulus plagioclase. The G-IX pyroxenite is not the only sequence in the Bushveld layered succession in which reversals of normal fractionation trends are evident, several others having been identified by Eales *et al.* (1990, 1991) in orthopyroxenites within the Lower and Critical Zones of the western Bushveld.

In the Lower and Lower Critical Zones, the reversals described by Eales *et al.* (1990, 1991) occur in the upper parts of thick accumulations of pyroxenite, and culminate with the deposition of olivine cumulates. Higher up, in the Upper Critical Zone, ultramafic cumulates displaying reversals rest directly on anorthositic footwall lithologies. A common feature of reversals of fractionation trends in the Lower and Critical Zones is the inclusion of corroded plagioclase grains in orthopyroxene and olivine (Eales *et al.*, 1991). Eales *et al.* (op. cit.) related the fractionation reversals in the Lower and Critical Zones, and their associated textures, to progressive influx and mixing of new liquid with resident liquids containing liquidus plagioclase. Reversals of the Mg# trend of orthopyroxene in the Lower and Critical Zones are not accompanied by reversed fractionation trends in plagioclase, or by a strong correlation between Mg# and Cr_2O_3 in pyroxene (Eales *et al.*, 1990), This contrasts with the parallel trends of Ca in plagioclase, and the Mg# and Cr_2O_3 content in the pyroxenes, in the G-IX pyroxenite.

Reversals in Mg# trends towards the tops of pyroxenite units overlain by olivine cumulates, similar to those in the Lower and Lower Critical Zones of the Bushveld, also occur in the Ultramafic Sequence of the Great Dyke in Zimbabwe, where they have similarly been attributed to influxes of new magma (Wilson, 1982). Decoupling of pyroxene Mg# and Cr_2O_3 trends in the Great Dyke has been attributed by Wilson (op. cit.) to scavenging of chromium by chromite, which is ubiquitous in olivine-bearing lithologies.

In the Eastern Layered Series of the Rhum Complex, reversed fractionation trends are displayed by olivine in layered troctolites overlain by peridotite layers. This has been attributed to compositional convection, in which there is an exchange of dense, primitive peridotite liquid with the intercumulus fluids in the upper parts of the underlying, partially crystallized, troctolites (Palacz and Tait, 1985; Tait, 1985; Tait and Kerr, 1987). The reversal in the trend of forsterite content in olivine is not parallelled by variations in the Ni content of olivine. Plagioclase compositions in the Rhum troctolite display wide within-sample ranges, and do not correlate with variations in the forsterite content olivine (Tait, 1985). The difference between plagioclase in the Rhum troctolites and the G-IX pyroxenite is that it is cumulus in the former.

Wide variations in Mg# relative to Cr_2O_3 content of pyroxenes of the G-IX pyroxenite, particularly in augite, may be indicative of the dominance of postcumulus trapped liquid shift (Barnes, 1986) over fractionation. The correlation between iron-enrichment and residual porosity predicted by the trapped liquid shift model is, however, not evident. The parallel reversed fractionation trends of the Mg# and Cr_2O_3 content of pyroxene and the Ca content of plagioclase are further arguments against trapped liquid shift. Another problem with the trapped liquid shift hypothesis is the sharply defined chemical breaks between one cycle and the next, which would imply rapid and complete solidification of one cycle before the accumulation of the subsequent cycle.

The sharp inflections in mineral chemical parameters at boundaries between cycles in the G-IX pyroxenite suggest that each cycle is the result of a discrete sequence of processes. It would seem logical, therefore, to ascribe the initiation of each cycle to a rejuvenation of the magma chamber, either by injection of fresh magma, or by convective

overturn of magma already in the chamber. The question of whether cyclicity is due to convective overturn or successive injections of fresh magma is weighed in the favour of multiple injections by a variety of factors. Primarily, the G-IX pyroxenite is isolated within relatively evolved gabbronorites, and convective overturn would therefore have had to take place, five times, within the 10 m thickness of magma from which the pyroxenite layer crystallized. Furthermore, the pyroxenite is laterally discontinuous, indicating channelled flow of intruding magma. Limited lateral as well as vertical extent of the pyroxenite places further limits of the volume of liquid available for convective overturn.

The basal contact of the pyroxenite is sharp, and dips at 15°, parallel to layering in the host gabbronorites. This, together with indications of a truncated Fe-enrichment trend in the footwall gabbronorites of the pyroxenite (Fig. 2), suggests an erosional lower contact. A preponderance of embayed plagioclase and augite inclusions in large low-Ca pyroxene grains at the top of the pyroxenite indicates that the upper contact might also be erosional. In other words, the G-IX pyroxenite might be a sill-like intrusion into partly solidified gabbronorites in the upper part of the LMZ. Sill-like intrusion of magma into partly solidified cumulates has similarly been proposed by Bédard *et al.* (1985) to explain laterally discontinuous peridotite layers in troctolite cumulates of the Rhum complex, and has also been suggested by Lee and Butcher (1990) as a possible explanation of certain textural and Sr isotope features of the Merensky and Bastard reefs of the north-eastern Bushveld Complex.

Sill-like intrusion of new magma has several implications, one of which is thermal erosion of the partially consolidated cumulates over which the new magma flows. A model of thermal erosion, by komatiites, of the substrates over which they flowed was presented by Huppert and Sparks (1985), and has been applied to practical examples, especially in the greenstone belts of the Yilgarn Block of Western Australia, by a number of workers (e.g. Lesher, 1989; Hill *et al.*, 1990, 1995; Perring *et al.*, 1995). It has also been considered, with modifications, as a possible process accompanying the replenishment of partially crystallized magma chambers with hot, fresh magma (Bédard *et al.*, 1988; Eales *et al.*, 1988). As pointed out by Eales *et al.* (1988), footwall cumulates need not be raised to their liquidus temperature for erosional effects to become significant. Disaggregation by melting in intercumulus spaces, added to turbulence in the inflowing magma, would probably be adequate for significant entrainment of footwall material.

Within the komatiite sequences studied by Hill *et al.* (1995) and Perring *et al.* (1995), there are lenses and sheets of adcumulate dunite. Several aspects of the models proposed by these workers to explain features of the dunite adcumulates may be relevant to the interpretation of the G-IX pyroxenite. It is therefore appropriate to summarize the salient aspects of these models. Several of the dunite lenses show upward trends of increasing forsterite content of olivine, indicating crystallization in an open magmatic system (Hill *et al.*, 1995). In most cases, the base of the lens is orthocumulate, grading up into adcumulates in the centre, with orthocumulates once again at the top of the lens. Some lenses exhibit mineral, textural and compositional layering on scales of centimetres to metres. In conditions like these, where adcumulate and orthocumulate textures alternate on a scale of tens of centimetres, it is difficult to envisage adcumulates developing by postcumulus processes (e.g. Tait *et al.*, 1984; Morse, 1986).

As pointed out by Campbell (1987), adcumulates develop where conditions favour growth of existing crystals, rather than nucleation of new ones. This requires a very low degree of supercooling, as well as physical removal of the nutrient-depleted boundary layer around growing crystals. Both these conditions are met by vigorous turbulent flow of lava, only slightly above its liquidus temperature, over a bed of growing crystals at the floor of a komatiite lava channel (Hill *et al.*, 1995). Orthocumulates, by contrast, form when the rate of crystal nucleation is high relative to growth, as in a partially drained channel where heat loss through the top of the flow is rapid, or when a flow encroaches over a cold substrate. Orthocumulates may also develop in the laminar flow regime in the boundary layer between the centre of the flow and the top of a pile of accumulated crystals.

Apart from displaying reversed fractionation trends, the G-IX pyroxenite is evolved relative to pyroxenites in the LZ and CZ, most obviously in its orthopyroxene Mg#. The maximum Mg# in the G-IX pyroxenite is 0.738, compared with averages from the Brits area of 0.8087 in the Bastard Reef, and 0.7833 in the UG2 pyroxenite (Eales *et al.*, 1994). The mineralogy is also relatively evolved, with augite being a significant, and often volumetrically dominant, cumulus phase.

A simple explanation of reversed fractionation cycles, and of the relatively evolved character of the G-IX pyroxenite, lies in its location in the distal facies of the magma chamber. As a new influx of magma streamed into the chamber, it would become increasingly evolved with distance from its intrusive source, due to thermal erosion and assimilation of low melting temperature phases from the cumulates through which it flowed, coupled with removal, by crystallization, of high temperature phases, as has

been suggested by Perring *et al.* (1995) in the case of komatiites that have assimilated their footwall. The first liquids reaching the distal facies would therefore be relatively evolved. As inward streaming of magma continued, the magma would become increasingly insulated, by the crystallization products of the initial phase of the injection, and conductive warming of surrounding cumulates, from reaction with the cumulates through which they flowed. Each cycle in the pyroxenite might therefore be built up from progressively less evolved magma emanating from a separate, but sustained, magma recharge event. It is difficult to explain why the top of cycle V displays less Mg and Cr enrichment than do the underlying cycles, but it may be due to incorporation of evolved supernatant material. Being relatively evolved, the magmas from which the G-IX pyroxenite crystallized were unable to completely resorb entrained material, hence the ubiquitous presence of embayed grains of augite.

Texturally, the bases of cycles in the G-IX pyroxenite are orthocumulates, which is consistent with supercooling against relatively cool floor cumulates and/or laminar flow in the basal boundary layer of an influx of fresh magma. An exception is the base of cycle III, which is an adcumulate, and coincidentally exhibits less Fe-enrichment of pyroxenes than do the bases of other flows. This may be ascribed to influx of the magmas from which cycles II and III crystallized in relatively rapid succession, so that significant supercooling did not occur at the base of cycle III. Adcumulates in the centres of cycles are attributed to crystallization during periods of maximum magma flux, as suggested by Hill *et al.* (1995) for similar textures in dunite lenses in komatiites. Orthocumulates at the tops of cycles relate to the waning of the magma flux.

Conclusions

Located within the distal facies of the western Bushveld, and situated stratigraphically in the upper reaches of the Lower Main Zone, the G-IX pyroxenite layer is made up of five cyles, each displaying reversals of the normal fractionation trend for all mineral chemical parameters investigated. Reversals of normal fractionation are not uncommon in layered intrusive complexes, but it is unusual for all minerals, both cumulus and intercumulus, to display parallel reversals. The features of the G-IX pyroxenite can be explained by the open system behaviour of a magma chamber replenished by successive batches of fresh magma. Adcumulate intervals within the pyroxenite are ascribed to periods of sustained streaming of magma, whereas orthocumulate intervals relate to the waxing or waning stages of replenishment cycles. Thermal erosion of footwall cumulates by successive magma influxes is evident from the ubiquitous presence, within the G-IX pyroxenite, of partially resorbed grains of augite.

From this study, as well as work by Eales *et al.* (1991), it is evident that mineral populations in some cumulates may be allochthonous, for want of a better term. This, added to the possibility of crystallization of some cumulates in a regime of flowing magma, must be added to the processes cited by McBirney and Hunter (1995) as complications in the application of cumulate terminology.

Acknowledgements

Original access to drillcore material was provided by the management and geological staff of Lefkochrysos Platinum Mines Ltd, and Roger Scoon assisted with the selection of appropriate drill core material for sampling. Mike Gregory is thanked for instruction in SEM techniques. The data are published with the permission of Gencor Ltd., the current holders of the mining lease. This work was funded by a research grant from the University of Durban-Westville. Critical reviews by C. M. B. Henderson and an anonymous referee are gratefully acknowledged.

References

Barnes, S.J. (1986) The effect of trapped liquid crystallization on cumulus mineral compositions in layered intrusions. *Contrib. Mineral. Petrol.*, **93**, 524–31.

Bédard, J.H., Sparks, R.S.J., Renner, R, Cheadle, M.J. and Hallworth, M.A. (1988) Peridotite sills and metasomatic gabbros in the Eastern Layered Series of the Rhum complex. *J. Geol. Soc. London*, **145**, 207–24.

Campbell, I.H. (1987) Distribution of orthocumulate textures in the Jimberlana Intrusion. *J. Geol.*, **95**, 35–54.

Cawthorn, R.G., Meyer, P.S. and Kruger, F.J. (1991) Major addition of magma at the Pyroxenite Marker in the western Bushveld Complex, South Africa. *J. Petrol.*, **32**, 739–63.

Dunlevey, J.N. and Mitchell, A.A. (1994) MODEPLUS: a program for computer-assisted modal measurements. *Computers and Geosciences*, **20**, 369–93.

Eales, H.V., Field, M., de Klerk, W.J. and Scoon, R.N. (1988) Regional trends of chemical variation and thermal erosion in the Upper Critical Zone, western Bushveld Complex. *Mineral. Mag.*, **52**, 63–79.

Eales, H.V., de Klerk, W.J. and Teigler, B. (1990) Evidence for magma mixing processes within the Critical and Lower Zones of the northwestern Bushveld Complex, South Africa. *Chem. Geol.*, **88**, 261–78.

Eales, H.V., Maier, W.D. and Teigler, B. (1991) Corroded plagioclase feldspar inclusions in orthopyroxene and olivine of the Lower and Critical Zones, western Bushveld Complex. *Mineral. Mag.*, **55**, 479–86.

Eales, H.V., Botha, W.J., Hattingh, P.J., de Klerk, W.J., Maier, W.D. and Odgers, A.T.R. (1993) The mafic rocks of the Bushveld Complex: a review of emplacement and crystallization history, and mineralization, in the light of recent data. *J. Afr. Earth Sci.*, **16**, 121–42.

Eales, H.V., de Klerk, W.J., Teigler, B. and Maier, W.D. (1994) Nature and origin of orthopyroxenites in the western Bushveld Complex, in the light of compositional data. *S. Afr. J. Geol.*, **97**, 399–407.

Hill, R.E.T., Barnes, S.J., Gole, M.J. and Dowling, S.E. (1990) *Physical volcanology of komatiites*. Geol. Soc. Australia (W.A. Divn.), Excursion Guide Book 1, 100 pp.

Hill, R.E.T., Barnes, S.J., Gole, M.J. and Dowling, S.E. (1995) The volcanology of komatiites as deduced from field relationships in the Norseman-Wiluna greenstone belt, Western Australia. *Lithos*, **34**, 159–88.

Huppert, H.E. and Sparks, R.S.J. (1985) Komatiites I: eruption and flow. *J. Petrol.*, **26**, 694–725.

Kruger, F.J. (1994) The Sr-isotopic stratigraphy of the western Bushveld Complex. *S. Afr. J. Geol.*, **97**, 393–8.

Lee, C.A. and Butcher, A.R. (1990) Cyclicity in the Sr isotope stratigraphy through the Merensky and Bastard Reef units, Atok section, eastern Bushveld Complex. *Econ. Geol.*, **85**, 877–83.

Lesher, C.M. (1989) Komatiite-associated nickel sulfide deposits. In: *Ore deposition associated with magmas: Reviews in Economic Geology*, **4** (J.A. Whitney and A.J. Naldrett, eds.), Soc. Econ. Geol., 45–101.

Maier, W.D. and Mitchell, A.A. (1995) Grain-size variations of cumulus plagioclase in the Main Zone of the Bushveld Complex. *Eur. J. Mineral.*, **7**, 195–204.

McBirney, A.R. and Hunter, R.H. (1995) The cumulate paradigm reconsidered. *J. Geol.*, **103**, 114–22.

Meyer, C. (1969) *Some petrological aspects of mafic rocks from four borehole sections between the Merensky Reef and the Main Zone gabbro in the western and eastern Bushveld Complex.* Unpubl. M.Sc. thesis, Potchefstroom University, 91 pp.

Mitchell, A.A. (1986) *The petrology, mineralogy and geochemistry of the Main Zone of the Bushveld Complex at Rustenburg Platinum Mines, Union Section.* Unpubl. Ph.D. Thesis, Rhodes Univ. 122 pp.

Mitchell, A.A. (1990*a*) The stratigraphy, petrography and mineralogy of the Main Zone of the northwestern Bushveld Complex. *S. Afr. J. Geol.*, **93**, 818–31.

Mitchell, A.A. (1990*b*) The Main Zone of the southwestern Bushveld in the vicinity of Brits. *Geol. Soc. S. Afr., Geocongress '90, Abstracts*, 419–22.

Mitchell, A.A. and Scoon, R.N. (1991) Discussion on 'the stratigraphy of the Bushveld Complex': a reappraisal and the relocation of the Main Zone boundaries. *S. Afr. J. Geol.*, **94**, 183–7.

Morse, S.A. (1986) Convection in aid of adcumulus growth. *J. Petrol.*, **27**, 1183–214.

Palacz, Z.A. and Tait, S.R. (1985) Isotopic and geochemical investigation of unit 10 from the Eastern Layered Series of the Rhum Intrusion, northwest Scotland. *Geol. Mag.*, **122**, 485–90.

Perring, C.S., Barnes, S.J. and Hill, R.E.T. (1995) The physical volcanology of Archaean komatiite sequences from Forrestania, Southern Cross Province, Western Australia. *Lithos*, **34**, 189–207.

Quadling, K. and Cawthorn, R.G. (1994) The layered gabbronorite sequence, Main Zone, eastern Bushveld Complex. *S. Afr. J. Geol.*, **97**, 442–54.

Robinson, P., Ross, M., Nord, G.L. Jr., Smyth, J.R. and Jaffe, H.W. (1977) Exsolution lamellae in augite and pigeonite: fossil indicators of lattice parameters at high temperature and pressure. *Amer. Mineral.*, **62**, 857–73.

Scoon, R.N. and Mitchell, A.A. (1994) Discordant iron-rich ultramafic pegmatites in the Bushveld Complex and their relationship to iron-rich intercumulus and residual liquids. *J. Petrol.*, **35**, 881–917.

Scoon, R.N. and Teigler, B. (1994) Platinum-group element mineralization in the Critical Zone of the western Bushveld Complex: I. Sulfide-poor chromitites below the UG-2. *Econ. Geol.*, **89**, 1094–121.

Sharpe, M.R. (1985) Strontium isotope evidence for preserved density stratification in the main zone of the Bushveld Complex, South Africa. *Nature*, **316**, 119–26.

Tait, S.R. (1985) Fluid dynamic and geochemical evolution of cyclic unit 10, Rhum, Eastern Layered Series. *Geol. Mag.*, **122**, 469–84.

Tait, S.R. and Kerr, R.C. (1987) Experimental modelling of interstitial melt convection in cumulus piles. In: *Origins of igneous layering* (I. Parsons, ed.) D. Reidel, Dordrecht, 569–87.

Tait, S.R., Huppert, H.E. and Sparks, R.S.J. (1984) The role of compositional convection in the formation of adcumulate rocks. *Lithos*, **17**, 139–46.

Wager, L.R. and Brown, G.M. (1968) *Layered igneous rocks.* Edinburgh, Oliver & Boyd: 588 pp.

Wilson, A.H. (1982) The geology of the Great 'Dyke', Zimbabwe: the ultramafic rocks. *J. Petrol.*, **23**, 240–92.

[*Revised manuscript received 10 July 1995*]